KfK 3541
Juli 1983

Electromagnetic Calorimeters Using Wire Chambers

J. Engler
Institut für Kern- und Teilchenphysik

Kernforschungszentrum Karlsruhe

KERNFORSCHUNGSZENTRUM KARLSRUHE

Institut für Kern- und Teilchenphysik

KfK 3541

Electromagnetic Calorimeters using Wire Chambers

Joachim Engler

Kernforschungszentrum Karlsruhe GmbH, Karlsruhe

Kernforschungszentrum Karlsruhe GmbH
ISSN 0303-4003

Electromagnetic Calorimeters using Wire Chambers

ABSTRACT

The situation of electromagnetic calorimeters using wire chambers or wire tubes is reviewed, and the specific properties of these gaseous calorimeters are described. In particular, the performance with respect to energy and spatial resolution is discussed. Recent developments gave remarkable improvements which make wire chamber calorimeter a promising choice for future application, especially for large scale detectors.

Elektromagnetische Kalorimeter mit Drahtkammern

ZUSAMMENFASSUNG

Es wird ein Überblick über die Situation elektromagnetischer Kalorimeter gegeben, die Drahtkammern oder Drahtröhren verwenden und die speziellen Eigenschaften dieser Gaskalorimeter werden beschrieben. Insbesondere werden Energie- und Ortsauflösung diskutiert. Jüngste Entwicklungen ergaben bemerkenswerte Verbesserungen, die Kalorimeter mit Drahtkammern in zukünftigen Anwendungen sehr vielversprechend erscheinen lassen, insbesondere bei modernen Großdetektoren der Teilchenphysik.

Invited talk at the Vienna Wire Chamber Conference, February 15-18, 1983

1. INTRODUCTION

Since the last Vienna conference 3 years ago, a new and wide field of applications of wire chambers has opened up, namely in electromagnetic calorimeters, predominantly used in high energy physics, but also in related disciplines. In the late seventies, wire chambers were used only sporadicly in calorimetry, e.g. for positron measurements in the maximum of a shower. But they seem now to become the most commonly used technique for large scale detectors.

Electromagnetic calorimeters are mainly used to determine the energy, but also the spatial positron and the direction of an incoming electron or photon. In addition, particle identification is possible in the sense that electrons and photons can be efficiently distinguished from hadrons or throughgoing muons.

In a calorimeter, the total particle energy is degraded in a block of matter into measurable atomic ionization and excitation. The calorimeter performance improves with increasing energy, because the fluctuations in the cascade process become less and less important due to the higher number of secondary processes.

Best results are obtained if a homogeneous detector is used, for which the absorbing block and the active material which detects the shower particles are identical. With the advent of large scale detectors, however, this ideal technique became prohibitive, mostly because of cost limitations. Nevertheless, large scale experiments with 4π solid angle coverage use homogeneous detectors. Well-known examples are the Crystal Ball (NaI), the Plastic Ball (plastic scintillator) or the JADE lead glass calorimeter.

In most partical cases calorimeters are realized by utilizing a sampling method. In these calorimeters the cascade develops in a dense material and the ionization is sampled in slices of an active material interspersed in the absorbing block. As the active material one often uses a scintillator. The first calorimeters used this technique, and still

today many calorimeters are built with scintillators. Recent examples for large scale applications are the UA1 and UA2 calorimeters at the SPS collider or the ARGUS detector at DORIS. Many detector systems, however, use ionization chambers, namely liquid and gas ionization chambers.

As to liquid ionization chambers, the only fluid used so far is liquid Argon (LAr). The problem encountered with other liquids is - similar to gas counters - the electron attachment: Free electrons are lost by formation of negative ions, which move too slowly. Only the noble gases Ar, Kr, Xe and CH_4 give reasonable charge output. Despite of attractive properties like good energy resolution, simple absolute calibration, and stable operation, the necessity of a cryostate and the complication of cryogenics have led LAr calorimeters to be used only in a few systems.

Many large scale calorimeters use or will use gaseous wire chambers as active devices. Wire chambers offer many advantages, and the motivation for using them is distinct from one detector to the other. But amongst the most obvious reasons are the following:

a) the possibility of a fine spatial segmentation in 3 dimensions,
b) a good efficiency for low energy electrons and photons,
c) low costs,

and last, but not least, the fact that the physicist community has more than half a century of experience with gas detectors since Geiger's invention in 1912.

Since on this conference calorimetry is a rather new subject, I will briefly review some of the fundamental aspects in electromagnetic cascade processes for those who are not so familiar with this subject. I will also recall - at least to some extent - what happened in the last three years in this new field of wire chamber applications.

2. SHOWER FLUCTUATIONS

In order to give a first impression of how shower fluctuation in reality looks like, two Monte Carlo generated cascades[1] are shown as an illustration in Fig. 1. The cascades are generated with the EGS code[2] in a sampling calorimeter consisting of 1/3 X_o lead plates interleaved with 10 mm gas gaps. For an understanding of the properties of wire calorimeters, we shortly have to discuss the underlying fluctuations in a cascade. A more thorough and detailed treatment can be found in the review articles of U. Amaldi[3] and S. Iwata[4].

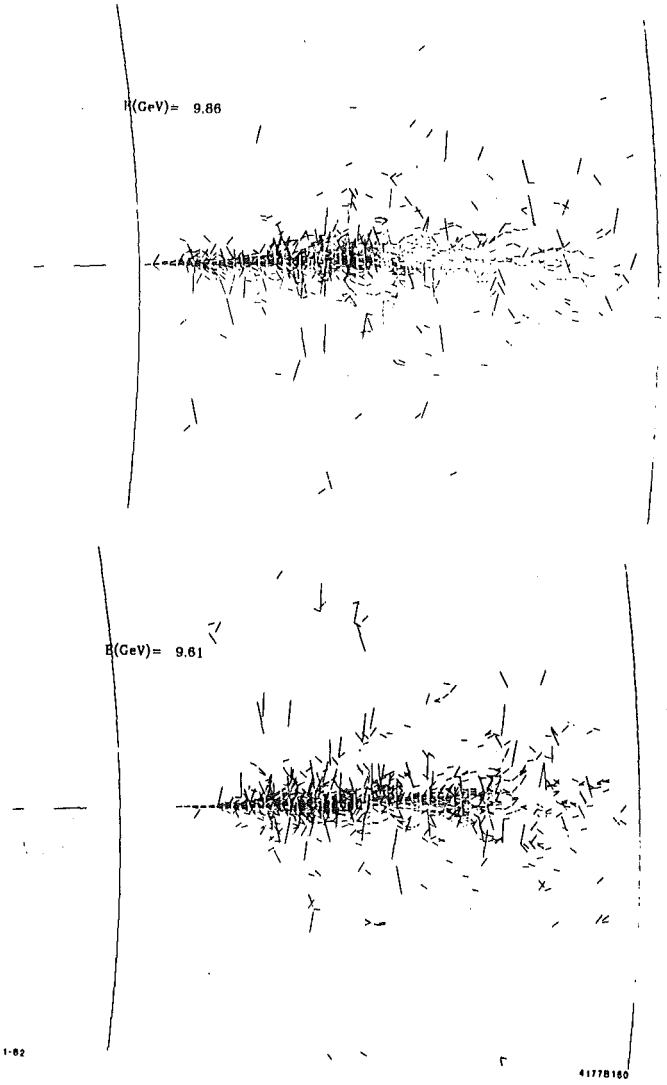

Fig. 1
Two Monte Carlo generated photon showers in a sampling calorimeter. The figure is taken from Ref. 1.

The longitudinal propagation of a cascade is governed by the radiation length X_o, whereas the lateral spread is determined by the Molière radius R_M. Both units are material constants and the proper scaling varies when changing from one absorbing material to the other.

For a homogeneous detector the measured signal is proportional to the sum of the deposited energy of all charged tracks, which is often called the "total track length" T. This quantity depends on the minimum detectable energy of an electron in the detector which is usually called the cut-off energy E_c. This threshold energy depends on the detector type and its operation and shortens the total track length as seen by the detector. In addition, T depends on the critical energy ε in the absorbing material. ε is the energy of an electron at which its energy loss in ionization collisions equals that in radiation processes. Roughly speaking, the multiplication process in an electromagnetic cascade stops when the electrons and positrons are slowed down to the critical energy, and they continue to lose their energy only in collision losses. If $E_c = 0$, i.e. electrons and positrons are measured down to zero kinetic energy, the total track length - when measured in radion length - can be written to a first approximation as

$$T/X_o = E/\varepsilon \quad . \tag{1}$$

X_o and ε are both material constants and therefore T is proportional to the incident energy E. This makes calorimetry possible. In a homogeneous detector, fluctuations enter in case of a finite cut-off energy. As an example, the Cerenkov light emission in Pb-glass cuts off at 0.5 MeV kinetic energy. A Monte Carlo calculation[5] gives for the reduction factor F of the total track length $F = 0.88$. A similar calculation[6] gives $F = 0.65$ for $E_c = 1.0$ MeV in lead. The intrinsic limit on energy resolution comes from this cut-off. In NaI and BGO crystals the shower electrons are detected down to a kinetic energy of a few keV and the resolution is limited only by detector imperfections, but not by shower fluctuations. Anyhow, a finite cut-off energy limits the performance only little. Longo and Sestili[5] have computed for the intrinsic energy resolution in Pb-glass a very low value, namely

$$d\sigma(E)/E = 0.7\%/\sqrt{E(GeV)} \quad .$$

Let us now turn to sampling calorimeters. Limitations due to a finite cut-off energy in the counter become negligible with respect to the fluctuations caused by the sampling method. It is customary to distinguish between to classes of calorimeters differing in their detection mechanisms: "Digital calorimeters" and "proportional calorimeters". In digital devices, only the number of tracks traversing the gaps between the sampling planes are counted irrespective of the individual length of the track and the energy deposited in it. In proportional calorimeters, also the energy of the electrons and positrons traversing the gap is measured and summed up to a total signal.

2.1 Digital Calorimeters

When using sampling plates of a thickness x, the total track length is cut into N individual tracks, and we can write for the number N of tracks as seen in the sampling gaps:

$$N = T/x = E/\varepsilon \cdot 1/t \quad . \tag{2}$$

$t = x/X_o$ is the sampling thickness measured in radiation length. Applying Poisson statistics, we obtain for the energy resolution

$$\sigma(E)/E = 1/\sqrt{N} = \sqrt{\varepsilon} \cdot \sqrt{t/E} = 3.2\sqrt{\varepsilon(MeV)} \cdot \sqrt{t/E(GeV)} \quad . \tag{3}$$

These fluctuations due to track-counting are often called sampling fluctuations. We have assumed all gap crossing to be independent. This is not valid for very fine sampling steps, but holds for all practical cases down to approximately $1/10\ X_o$.

From eq. (3) is seen that in order to obtain a good energy resolution one has to choose an absorbing material with a low critical energy. Values for ε of typical materials are given in Table 1.

Table 1: Critical energy ε for typical absorbing materials

Material	Al	Ar	Fe	Cu	W	Pb	U
ε (MeV)	39.3	29.8	20.5	18.7	7.9	7.2	6.6

In most cases, Pb is used. Uranium gives no major improvement, but if Fe has to be chosen (for instance when magnetic flux iron acts as the absorber), the energy resolution worsens by about 70%.

The rough estimate of eq. (3) has to be refined in real calorimeters for several effects among which the following two dominate:

a) A finte cut-off energy reduces the number of tracks like in a homogeneous detector by a factor $F(E_c/\varepsilon)$.
For many detectors E_c = 1 MeV is a reasonable assumption, that means F = 0.65.

b) Multiple scattering spreads out the shower particles, especially for high Z absorbers. If the angle of the electrons with the shower axis is θ, the sampling plate to be traversed becomes thicker by 1/cos θ. Fischer[7] has calculated by a MC method for the mean angle of all cascade particles: $\langle\cos\theta\rangle = 0.57$.

Filling both values into eq. (3) one arrives at the energy resolution in a Pb calorimeter in a first approximation

$$(4) \qquad \sigma(E)/E_{sampling} = 13.7\% \sqrt{t/E(GeV)} = \sqrt{1/53}\ \sqrt{t/E} \ .$$

For a quick estimate we see that the sampling fluctuations behave like N = 53 uncorrelated tracks in a 1 GeV shower for t = 1.

Four examples for digital calorimeters are listed in Table 2. The two

	Sampling		Detector		Energy Resolution		Energy Range	Non Linearity	Reference
	X/X_o	X total	Cell Size (mm)	Operation mode	σ/E	$\sigma x \sqrt{E}.t$	(GeV)		
1)	0.29	8.0	4	flash tube optical read-out	$0.08/\sqrt{E}$	.15	0.15...05		(8)
2)	0.9	13.0	3.5 x 5		$.12/\sqrt{E}$	.13	0.5....4	∿10%, 4 GeV	(9)
3)	0.9	14.5	9 x 9	limited streamer	$\sim .26/\sqrt{E}$	.27	4...10	∿ 6%, 10 GeV	(10)
4)	0.9	14.5	6 x 9		$\sim .26/\sqrt{E}$	.27	10	∿10%, 24 GeV	(11)

TABLE 2: Calorimeters with digital read-out

flash tube calorimeters have both very small cell sizes of about 4 mm and indeed reach the estimated resolution of eq. (4). The group of Conversi and coworkers[9] has tested its calorimeter up to 4 GeV. A disadvantage of digital calorimeters is that at energies above a few GeV they saturate due to the higher track density near the axis of the shower. Both streamer tube calorimeters of Jarocci and coworkers were tested at higher energies and with a coarser cell size. It is not surprising that due to both effects they do not reach the intrinsic energy resolution. But the linear energy response has been pushed to rather high energies. Up to 24 GeV, the non-linearity is only 10%. The effective cell size is given laterally by the tube cross section and along the tube by the streamer obscuration length which is the minimum distance between two independent streamers. The authors estimate it to be $\sim$ 1.5 mm.

Digital calorimeters have found wide application for massive calorimeters in neutrino experiments, e.g. the FNAL flasch tube detector[12] and nucleon decay experiments, e.g. the NUSEX experiment operating in the Mt. Blanc tunnel[13].

2.2 Analogue Calorimeter

In a proportional calorimeter also the deposited energy of a track and its length is measured. Both effects imply additional sources or fluctuations, namely:

a) Landau fluctuations, i.e. the statistical fluctuations of δ-ray emission and

b) path length fluctuations, i.e. low energy electrons are spread out at large angles with respect to the shower axis and travel long distances in the active gap (see Fig. 1).

While contributing minor corrections to the sampling fluctuations in the case of solid or liquid detectors, both effects dominate in gas proportional calorimeters unfortunately. For the Landau fluctuations this is obvious because of the much smaller density of a gas-filled sampling gap.

As to the path length fluctuations, these are much larger in gas than in solid material for two reasons:

1) The cut-off energy in gaseous chambers is usually much smaller and the contribution of low energy electrons which deposite much more energy when travelling along a sensitive layer is more pronounced. Long tracks of such low energy electrons - especially outside the kernel of the cascade - can be seen in Fig. 1.

2) In gas the multiple scattering is much smaller and an electron once moving in a gap stays in it, whereas a dense layer tends to scatter it back into the absorber plates.

Both effects are since long a well-known drawback and many ideas have been proposed to cure it. Fischer was the first who calculated the effect quantitatively by using a modified version of the EGS code. His results for the energy resolution are reproduced in Fig. 2a. In the cal-

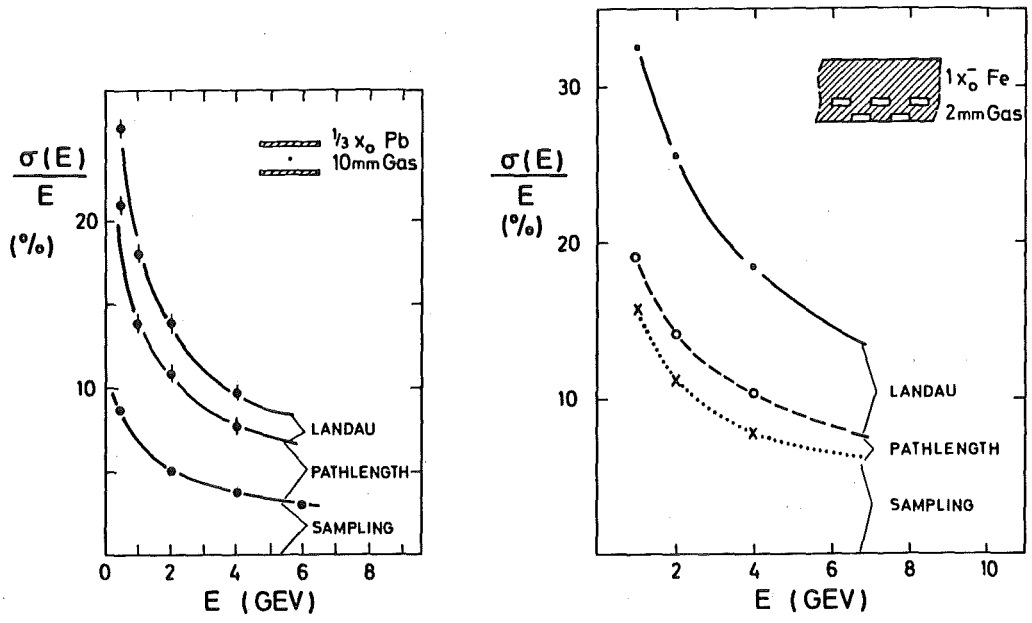

Fig. 2: Monte Carlo calculation of the energy resolution in sampling calorimeters using

a) wire chambers - Ref. 7,

b) wire tubes - Ref. 14.

culation, a sampling calorimeter with lead plates of 1/3 X_o interleaved with 10 mm thick multiwire proportional chambers was used. As can be seen, Landau and path length fluctuations contribute to a large extent to the deterioration of the energy resolution when compared with mere sampling fluctuations.

An obvious remedy to reduce the path length fluctuations is to cut on those tracks which have a too high inclination with the shower axis and travel too far from it. By using proportional tubes instead of planar wire chambers, the bulk of δ-rays is cut automatically by the tube walls, and electrons are allowed to elongate from the shower axis in one direction only. The effect is clearly demonstrated by a MC calculation performed by T. Lundlan et al.[14] who compare planar wire chambers with tube configurations. The results for the tube configuration (Fig. 2b) show that the relative contribution of the path length fluctuation is effectively reduced. This is one reason why in many calorimeters arrays of proportional tubes are used.

A remedy to reduce also the Landau fluctuations has been proposed by Atac et al.[15]. They operate the proportional tube system under high voltage in a partially saturated gain. Under these circumstances, a high density of ionization causes gain saturation due to positive ion shielding around the wire. Consequently the large pulse heights in the Landau tail are reduced and in fact a more symmetric pulse height distribution is obtained. When plotting the energy resolution of the calorimeter with respect to the high voltage applied, the authors observe a minimum (see Fig. 3) before the limited streamer mode sets in. The improvement with respect to the fully proportional mode is in the order of 10%. On the other hand, the operation in a partly saturated gain causes unlinearities of the calorimeter response at high energies. The authors of Ref. 15 found an unlinearity of 6% for showers of 50 GeV primary energy.

Similar observations are reported by the authors of Ref. 14, who obtained an improvement of 15% at the expense of a non-linearity that sets in beyond 10 GeV. The authors studied the energy resolution also in more

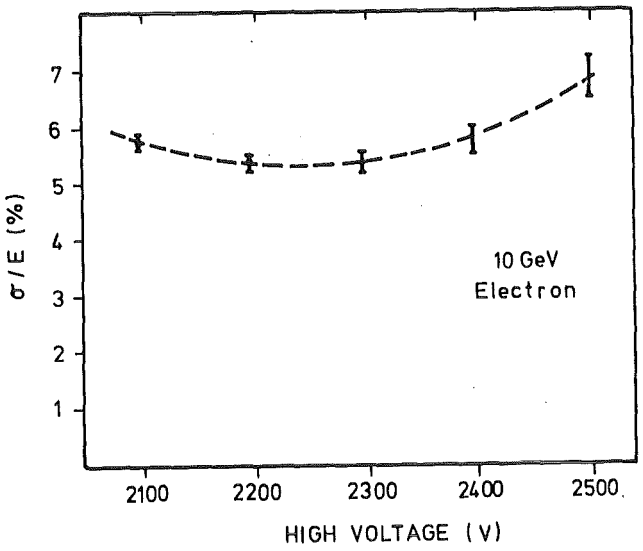

Fig. 3:

The energy resolution in a wire tube calorimeter versus high voltage - Ref. 15.

detail by MC calculations. The energy response of the calorimeter could be reproduced when imposing a single wire saturation function that was folded into the MC calculation. The saturation function had been obtained experimentally by illuminating a single wire with radioactive sources. Also the ALEF collaboration observed an improvement in the energy resolution of 10 - 15% when operating their test calorimeter for the LEP detector in the saturated avalanche mode. The final gas gain of approximately 10^4 will be a compromise between a reasonably good energy resolution and a small unlinearity at the highest energies.

A compilation of calorimeters operated in a proportional mode is given in Table 3. Positions 1-9 give reslts on test devices. The scaled energy resolutions scatter around $0.30 \cdot \sqrt{E/t}$. One observes that calorimeters with tubes do not obtain a significant improvement on the energy resolution, most likely because the lateral dimensions used are too wide to cut efficiently on spread-out electrons. The test calorimeter using very small tubes sizes (pos. 8) has iron as absorber and cannot be compared directly. If one scales the result of this calorimeter according to the critical energy of iron, one obtains from the extrapolation a rather low value for the energy resolution of $0.20/\sqrt{E}$.

	x/X_0	X^{total}	Detector Type Dimensions (mm)	Operation	Energy Resol. σ/E	$\sigma \cdot \sqrt{E}/E$	Range (GeV)	Reference
1.	.68	27	chamber, 10	prop.gain = 780	$.24/\sqrt{E}$	.29	10...24	(16)
2.	.23	13.5	chamber, 4	proport.	$.15/\sqrt{E}$	.29	.5...12	TPC-EC (17)
3.	.23	11.3	tube, 30x12	"	$.025 + .15/\sqrt{E}$	.31	.5...3.2	CLEO-Proto (18)
4.	.50	18	Al tube, 10x10	"	$.17/\sqrt{E}$	.24	.5...15	MAC-Proto (19)
5.	.41		brass tube,6x11	"	$.22/\sqrt{E}$	.34		test (15)
6.	.51	20	plastic tube, 7x10	"	$.24/\sqrt{E}$	.30	10...40	FNAL-Proto (20)
7.	.8	16	Al tube,10x10	prop.,low gain	$.01 + .20/\sqrt{E}$	.24	2...50	FNAL-Proto (21)
8.	1.(Fe)	20	tube, 2x5	saturat. prop.	$.33/\sqrt{E}$	.33	1...6	Magn. Pole-Proto (14)
9.	.50	17	Al tube, 10x10	"	$.162/\sqrt{E}$	.23	2...17	MAC-Proto (15)
10.	.41		brass tube,6x11	"	$.17/\sqrt{E}$	.26	10	test (15)
11.	.27	12	tube, 32x12	proport.	.065	.28	Bhabhas and $\gamma\gamma$ at 5 GeV	CLEO operation (22)
12.	.50	18	tube, 20x10	"	.08	.43	Bhabhas at 14.5 GeV	MAC operation (23)

Table 3: Proportional Wire Calorimeters

The last two rows give the energy resolution for the full detector operation for the CLEO and MAC detectors. CLEO can reproduce its test results with elastic (Bhabha) scattered electrons of 5 GeV. The MAC collaboration would expect a resolution of 5% for the elastic electron peak at 14.5 GeV, but only 8% are observed. The difference is attributable to scattered non-functioning channels, about 5% in total. It might also reflect the difficulty to maintain stable operation and calibration of a large detector system for a long period of time. This becomes more apparent at higher energies where the shower fluctuations are down to a few percent.

3. SPATIAL RESOLUTION

The intrinsic limitations in spatial resolution are given by the lateral spread of a shower which is mainly caused by multiple scattering of electrons that do not radiate but travel away from the axis. The shower spreads transversely with an exponential fall-off which becomes flatter for deeper longitudinal dephts. An example is shown in Fig. 4, as obtained by a wire tube calorimeter operating at the CERN SPS[24]. The proper scaling variable for the lateral distribution is the Molière radius. This unit is the rms spread of electrons of critical energy that have passed through one radiation length thickness and is given as $R_M = 21\ \text{MeV}/\varepsilon \cdot X_o$. In order to distinguish two adjacent showers and to measure their energy separately, they have to be one Molière radius apart. In a cylinder with a radius of 1 R_M approximately 90% of the total shower energy are contained and within 2 R_M about 95% are found. For materials with high Z the Molière radius is large due to the small critical energy and therefore the showers are wider transversely than in a low Z material. In compact lead the Molière radius is 1.5 cm which becomes larger when less dense sampling gaps are interspersed. In order to keep the Molière radius small, the calorimeter has to be as compact as possible to avoid too much overlap of contiguous showers.

In reality, the limitations on spatial resolution are of practical nature and have to do with the granularity of the calorimeter, both in

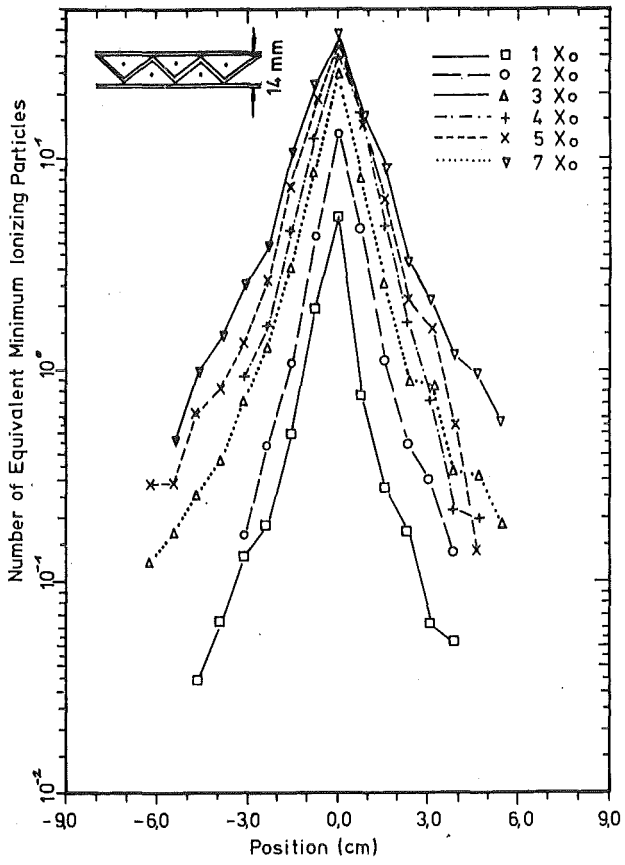

Fig. 4:

The lateral energy deposition in the first 7 radiation lengths - Ref. 24.

longitudinal and in transversal direction. It is in this spatial segmentation where wire chamber calorimeters reveal their superiority to most other copeting techniques, because a large number of individual cells can be read out without major complications.

The simplest way to find the position of a shower is to measure the centre-of-gravity of the lateral energy released. Due to the strong exponential decrease, this does not give the best estimate, and corrections have to be applied[25]. It does not give the best resolution either. Taking higher moments should improve the resolution since it weights the large signal channel more than the low signal channels. The authors of Ref. 20 tried position measurements taking the first, second and fourth moments of the lateral spread. The best results were obtained with the second moments, and no further improvement was observed when going to higher moments.

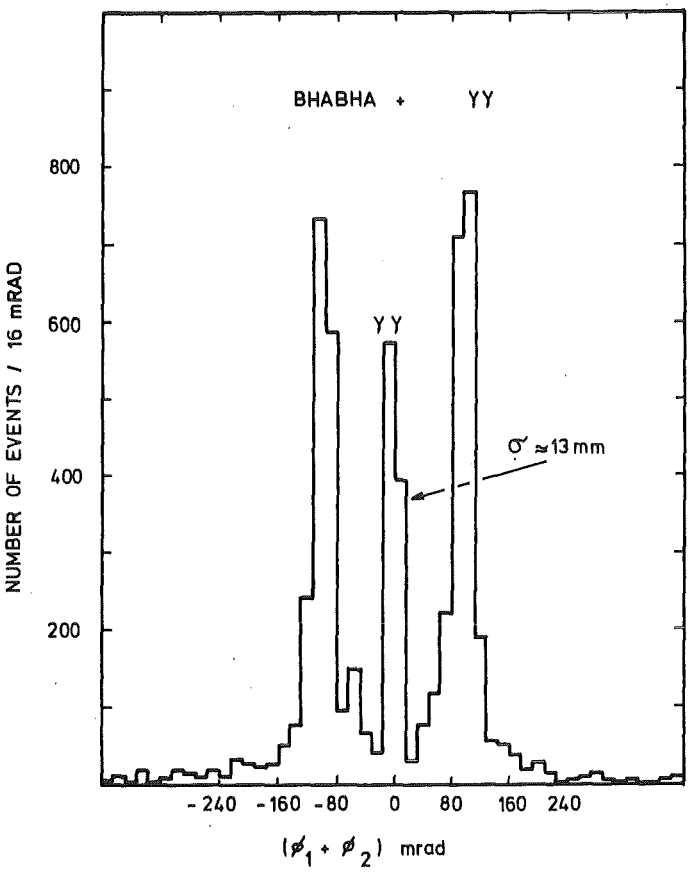

Fig. 5:

The position resolution obtained in the CLEO detector for two photons emerging from e^+e^- annihilation and for Bhabha scattering.

As an example for a position determination in a large scale detector the results in the CLEO calorimeter are shown in Fig. 5. Plotted is the difference in the azimuthal impact points of 2γ and Bhabha pairs emerging from e^+e^- interactions. The two photons emerge exactly back to back and give a narrow peak. The elastic scattered electrons and positrons are deflected in a magnetic field and are separated due to the bending angle. Having a tube width of 31 mm, the detector measures a resolution of 6 mrad corresponding to a rms resolution for the impact point of $\sigma = 13$ mm.

A few examples of calorimeters that aimed at a good position resolution are listed in Table 4. As can be seen, about 2 mm are achieved with strip widths of approximately 10 mm. The first calorimeter combines strip and pad read-out, whereas the second has read-out only on strips. The third calorimeter reads the wires in a tube layer, but the tubes are not individually read out. Instead, the signals from 16 adjacent channels are

	Segmentation	Position Resolution Impact Point	Shower Axis	Energy Range (GeV)	Ref.
1.	11 mm strips at 5 long.depths	3 mm	12 mrad at 30 GeV	10...40	(14)
	3x5 cm^2 pad. 3 long. segments	2 mm	20 mrad at 10 GeV		
2.	12 mm strips for 0...5.4 X_o	1 mm		10...45	(15)
	12 mm strips for 5.4...17.6 X_o	3 mm			
3.	10 mm wire tubes for 0...4.8 X_o	2.5 mm		2...50	(20)
	10 mm wire tubes for 4.8... 9.6 X_o	2.5 mm			
	10 mm wire tubes for 9.6...16 X_o	5.0 mm			

Table 4: Spatial Resolution in Wire Chamber Calorimeters

combined in a weighting technique using a resistive network and fet into three independent amplifiers reducing the number of read-out channels in this way by a factor of 5. The authors used quadratic weighting functions and extracted from the three signals the zeroth, first and second moments of the transverse energy distribution. Thus they obtained immediately the energy and the position of a shower and, with the second moment, an indication whether a signal belongs to a single gamma or originates from a π^0.

4. PERFORMANCE

4.1 Gain Stability

At high energies the cascade fluctuations limit the energy resolution only within a few percent, and in most calorimeters the final performance will be determined by a thorough calibration and stable operation, especially for large scale detectors where often 10^4 and more channels have to be operated reliably over periods of many months and even years.

A technical problem with gas calorimeter comes from variation in the gas amplification. The gas amplification A depends on the electric field E, the gas density ρ, the gas composition M and the temperature T. Usually one writes down the ansatz

$$\frac{\Delta A}{A} = K_1 \frac{\Delta E}{E} - \frac{\Delta \rho}{\rho} + K_3 \frac{\Delta M}{M} + K_4 \frac{\Delta T}{T} \tag{5}$$

and determines the constants K_i for the specific gas counter used and its operation conditions. Typically one finds $K_1 = 20$, $K_2 = 12$, $K_3 = 5$, $K_4 = 6$. Furthermore, A depends on mechanical tolerances like the sense wire radius, its displacement within the cell, dimensions of the cell, etc. To obtain a stable amplification within a percent is a challenge to each experimentalist working in calorimetry. Care has to be taken not only for local subgroups in a calorimeter but also for global uniformity of the response.

In a calorimeter non-operating channels have a stronger influence than in normal tracking devices. A non-responding amplifier systematically leads to a wrong measurement of the particle energy and not only to a less accurate one like in track chambers which have more redundant measurements on the track parameters.

Large proportional gas calorimeters, however, have already been operated successfully for periods of years, e.g. the proportional drift tubes of the CHARM collaboration[26] and the CLEO calorimeter[22]. High voltage, gas flow and gas composition can be controlled to the necessary precision of 10^{-3} and better. The remaining gain variations resulting e.g. from barometric pressure are permanently controlled by monitor tubes which are illuminated by radioactive sources.

Calibration is normally done with test beams and where possible with elastic scattering events. Also penetrating particles like muons or throughgoing pions are used as reference points.

4.2 Read-Out Techniques

In order to make full use of the possibility to segment wire chambers, read-out techniques have been developped that allow to read out space points rather than projections. If only the cathode itself is used to pick up the induced signal, the pattern is restricted to the chamber construction, and the cathodes must be designed carefully, so that the electrostatic field for the sense wires is not influenced by this pattern.

Resistive cathodes which are transparent for the r.f. signals allow to split the two functions of the cathode and separate the cathode of the chamber from the pick-up electrode for read-out purposes. Thereby all interference problems of the gas and high voltage system with the read-out system are avoided. In many designs the anode information is no longer used and read-out goes only via pick-up electrodes on the cathodes. For illustration, a typical construction is shown in Fig. 6.

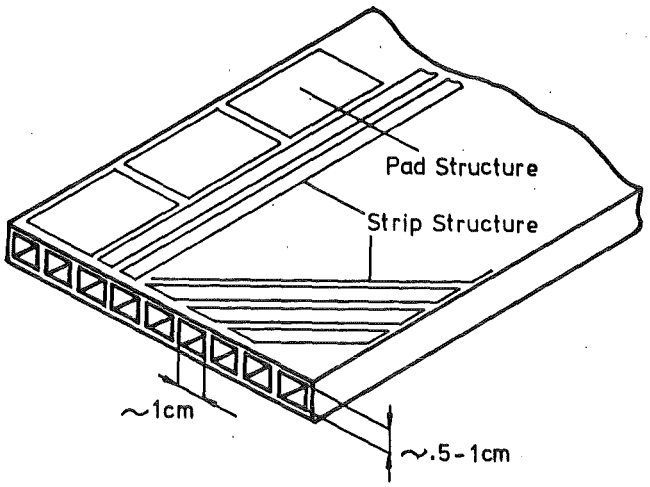

Fig. 6:
Principle of arrangement of wire tubes used in calorimetry.

In order to have reasonable transparency for typical geometries of strips and pads in the cm region, resistivitities of $2 \cdot 10^5$ Ω/sq are necessary. If smaller read-out patterns are desired, a higher resisitivity is needed to aboid a broadening of the amplitude distributions on contiguous channels. Two techniques for constructing resistive cathodes have been developped. The Frascati group[9] uses PVC plastic tubes coated with graphite, used for instance in the NUSEX experiment in the Mt. Blanc tunnel. Y. Hayashide et al.[20] have developped conductive plastics by mixing a certain amount of carbon power to it. They found a material with good mechanical rigidity and also high radiation resistivity. A resisitivity of up to 100 KΩ/sq was obtained.

5. NEW TECHNIQUES AND DEVELOPMENTS

In this chapter I would like to mention two new developments as examples among others which look very promising for the future.

5.1 Time Projection Calorimeter

Two groups[27,28] are developping calorimeters based on the time projection technique by drifting the ionization electrons in long channels

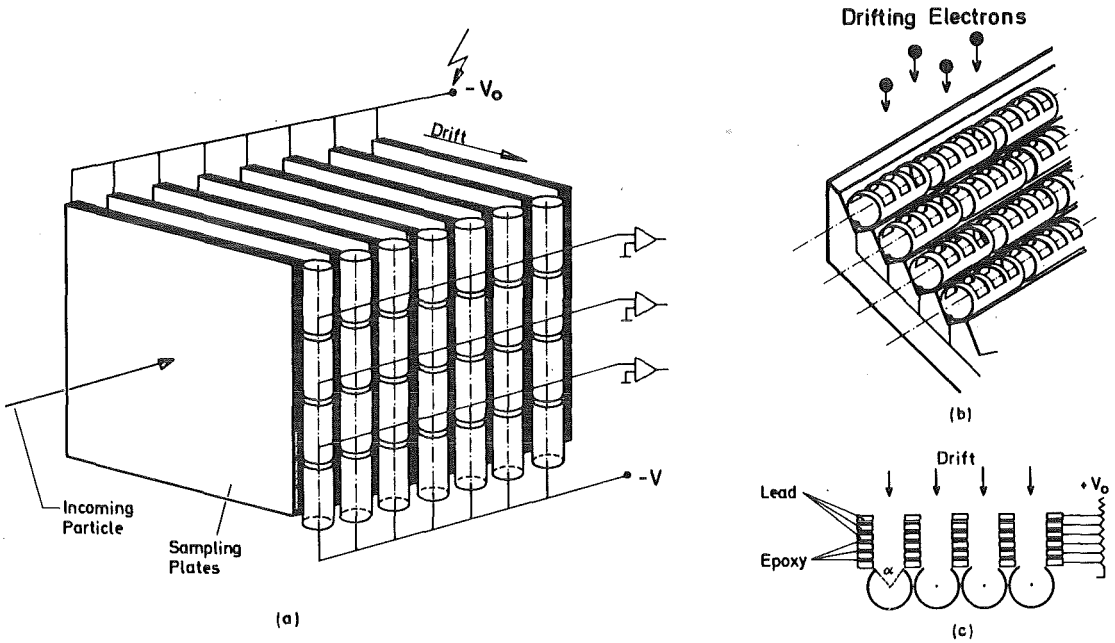

Fig. 7: The time projection calorimeter (TPC) as proposed for a LEP detector

a) Converter plates with pick-up chamber
b) Detail of tube lay-out with decoupling grid
c) Detail of the converter plate lay-out

embedded in the radiator material. The drift direction is perpendicular to the axis of the cascade and the electrons are detected by pick-up chambers at the ends of the drift channels. Read-out is performed in narrow time buckets so that a high spatial resolution and fine segmentation can be achieved with a modest number of read-out channels. The detailed information on the spatial structure of the shower can be used in an off-line analysis to suppress large ionization fluctuation, especially far away from the shower axis, to improve the energy and spatial resolution.

As a principle of a drift calorimeter, the proposed design for a LEP detector is shown in Fig. 7. The pick-up chamber on the side is layed-out as proportional tubes which are segmented lontigudinally. The

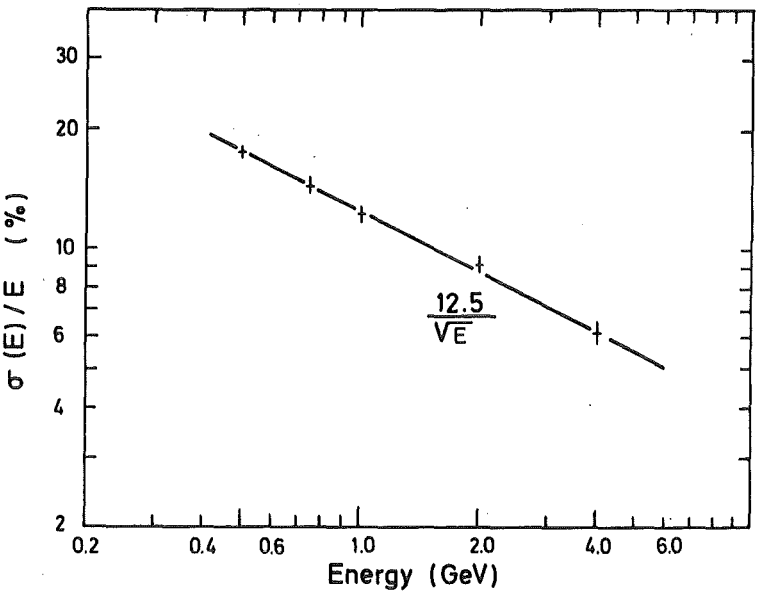

Fig. 8:

The energy resolution obtained in the CERN time projection calorimeter - Ref. 27.

tube wall acts as a pad read-out with a very good signal coupling of more than 90%.

Drifting over distances of 0.5 to 1.0 meter seems to imply no major problems. Attenuation lengths of 7.0 m [29] and 1.5 m [28] have been measured in a 10 mm drift gap with Ar/CO_2 gas. L.E. Price also investigated an exponential rising drift field which has the advantage to yield a focussing component that keeps the drifting electrons in the gap and obtained much longer attenuation lengths.

The measured energy resolution is $24\% \cdot \sqrt{t/E}$ for the CERN calorimeter and $23\% \cdot \sqrt{t/E}$ for the Argonne one. The energy dependence of the former is shown in Fig. 8. The spatial resolution is determined by the lay-out. In the drift direction time buckets of 100 µsec are easily possible with modern FADC's and will give a resolution of a few millimeters.

Drifting in a magnetic field causes no major difficulties as long as it is directed along the drift axis. In a recent test[30] the CERN-group succeeded in obtaining an improvement when operating the calorimeter in a 1.0 Tesla field. The energy resolution improved to $11\%/\sqrt{E}$, which is an off-line analysis is expected to improve further. This is, to the authors'

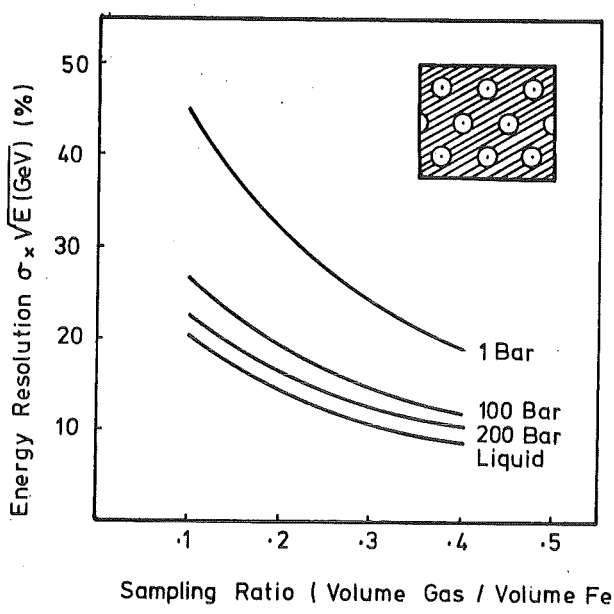

Fig. 9:

Monte Carlo calculation for energy resolution of a high pressure calorimeter - Ref. 31. The geometrical configuration is shown in the insert.

knowledge, the best resolution obtained so far for a gaseous calorimeter.

5.2 High Pressure Calorimeter

The other interesting development is followed by E. Rosso and coworkers[31] at CERN who investigate the performance of high pressure Argon tubes. The main intention is to have an elegant method to instrument the pole pieces of spectrometer magnets as active calorimeter elements. Steel tubes of 5 mm radius are filled with 200 bar Argon gas and permanently sealed. The ionization charge is collected on a concentric anode wire without charge amplification, that means in the ionization chamber mode. The gas density is one quarter of that of the liquid, and as a M.C. calculation for the energy resolution shows (see Fig. 9), the performance corresponds nearly to that of a LAr calorimeter. Recently, the authors have got encouraging results with zinc-plated carbon steel tubes by obtaining a long term stability over several months without observing a degradation of the charge output.

6. CONCLUSION

The above-mentioned examples are only two out of many other developments in wire chamber calorimetry. But already these two demonstrate how far the improvement in energy resolution can be pushed reaching almost the values obtained in calorimeters with dense active material. On the other hand, wire chambers have the possibility of an easy and cheap segmentation and the advantage of a very fine granularity. They therefore offer a very promising choice for future applications, especially in large scale detectors.

REFERENCES

1) From 'Proceedings of the SLC Workshop on the Experimental Use of the SLAC Collider'
SLAC-Report 247 (1982) 283

2) R.L. Ford and W.R. Nelson
SLAC-Report 210 (1978)

3) U. Amaldi
Phys. Scripta 23 (1981) 409

4) S. Iwata
DNPU-3-79 (1979) Nagoya University

5) E. Longo and I. Sestili
Nucl.Instr. & Meth. 128 (1975) 283

6) H.H. Nagel
Z. Physik 186 (1965) 319

7) H.G. Fischer
Nucl.Instr. & Meth. 156 (1978) 81

8) S. Mikamo
KEK Preprint 82-16 (1982)

9) L. Friderici et al.
Nucl.Instr. & Meth. 151 (1978) 103

10) G. Battistoni et al.
Preprint LNF-82/16 and 'Proceedings of the Intern. Conf. on Instrumentation for Coll. Beams', SLAC 250 (1982) 195

11) dito, private communication by C. Bosio and E. Iarocci

12) F.E. Taylor et al.
IEEE Trans. Nucl. Sci. NS-27 (1980) 30

13) G. Battistoni et al.
Frascati Report LNF-82/81 (P), submitted to Phys.Lett.

14) T. Ludlam et al.
Nucl.Instr. & Meth. 198 (1982) 233

15) M. Atac et al.
Fermilab Preprint FN-368 (1982), submitted to Nucl.Instr. & Meth.

16) M. Atac et al.
IEEE Trans. Nucl. Sci. NS-28 (1981) 500

17) C.D. Buchanan, private communication

18) J.J. Müller et al.
IEEE Trans. Nucl. Sci. NS-28 (1981) 496

19) R.L. Anderson et al.
IEEE Trans. Nucl. Sci. NS-25 (1978) 340

20) Y. Hayashide et al.
Tsukuba Univ. Preprint UTPP-1/82

21) C. Blocker et al.
'Proceedings of the Intern. Conf. on Instrumentation for Coll. Beam Physics', SLAC 250 (1982) 200

22) CLEO Collaboration
Rochester University Preprint CLNS 82/538

23) MAC Collaboration
'Proceedings of the Intern. Conf. on Instrumentation for Coll. Beam Physics', SLAC 250 (1982) 174

24) V. Artemiev et al.
contribution to this conference

25) G.A. Akopdjanov et al.
Nucl.Instr. & Meth. 140 (1977) 441

26) A.N. Diddens et al.
Nucl.Instr. & Meth. 176 (1980) 189

27) E. Albrecht et al.
'Proceedings of the Intern. Conf. on Instrumentation for Coll. Beam Physics', SLAC 250 (1982) 212
and CERN-Preprint EF 82-16 (1982)

28) L.E. Price
'Proceedings of the Intern. Conf. on Instrumentation for Coll. Beam Physics', SLAC 250 (1982) 206

29) O. Ullaland and E. Lillethun
private communication

30) A. Cattai et al.
contribution to this conference

31) M. Barranco-Luque et al.
'Proceedings of the Intern. Conf. on Instrumentation for Coll. Beam Physics', SLAC 250 (1982) 185